Compact Band-Stop Half-Mode Substrate Integrated Waveguide Filter based on a Broadside Coupled Open Split Ring Resonator

Juan Hinojosa, Marcello Rossi, Adrian Saura-Rodenas, Alejandro Alvarez-Melcon, *Senior Member,* IEEE, and Félix L. Martínez-Viviente

***Abstract*—A shunt *RLC* resonant circuit obtained from a broadside coupled open split ring resonator (BC-OSRR) is proposed. This BC-OSRR cell allows a parallel connection with planar waveguides. Hence, it has been applied to a half-mode substrate integrated waveguide (HMSIW) section. The analysis of the frequency response and electromagnetic field distribution of the HMSIW structure loaded with an appropriate BC-OSRR cell have shown two main behaviors. The first characteristic is a high-pass frequency response inherent to the HMSIW and the second is a transmission zero in the pass-band of the HMSIW, which is due to the resonance of the BC-OSRR cell. First- and second-order prototypes have been designed and fabricated. The measured band-stop HMSIW filters using BC-OSRR achieve a 3 dB stop-band bandwidth around 10% with more than 21 dB insertion loss. This BC-OSRR cell with low undesired radiation loss can be a new alternative for the implementation of compact band-stop filters in planar technology.**

***Index Terms*—Band-stop filter, half-mode substrate integrated waveguide (HMSIW), split ring resonator (SRR).**

I. Introduction

BAND-STOP filters play an important role in RF/microwave applications to reduce signals at unwanted frequencies [1]. As with other low-pass and band-pass filters, the requirements in terms of performance, power handling capability, size, weight and cost are increasingly stringent. A possible solution to meet these requirements is to develop metamaterial-inspired structures within a substrate integrated waveguide (SIW). SIWs and half-mode substrate integrated waveguides (HMSIWs) are guided waveguide planar transmission lines that have become popular in recent years for microwave and millimeter-wave applications [2]-[10]. The performance parameters of SIWs (HMSIWs) such as insertion loss, quality factor and power handling capability are better than for conventional microstrip and coplanar (CPW) transmission lines. SIW (HMSIW) technology is low cost and can be easily integrated with planar circuit technology. However, if a given component is not available in SIW (HMSIW) technology, transitions or adapters are needed to interface with other planar technologies. This leads to a size increase and performance degradation of the whole subsystem. To avoid this inconvenience, it is necessary to develop a wide range of components in SIW (HMSIW) technology similar to those in conventional planar technologies.

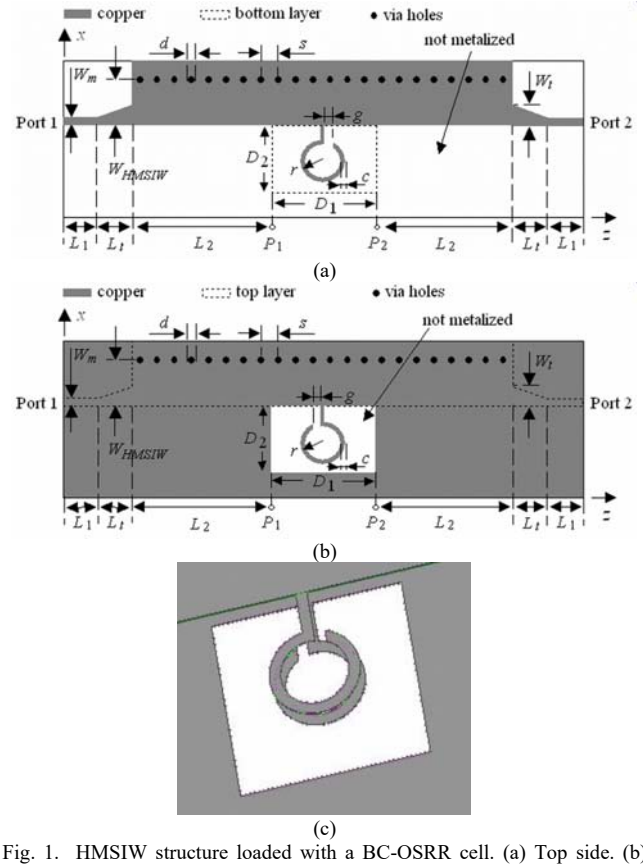

Fig. 1. HMSIW structure loaded with a BC-OSRR cell. (a) Top side. (b) Bottom side. (c) 3D view of the connection between the HMSIW and the BC-OSRR cell.

Manuscript received … This work was supported by the Spanish Ministerio de Economía y Competitividad, Fundación Séneca of Murcia and European Regional development funds under grants TEC2016-75934-C04-4-R and 19494-PI-14.

J. Hinojosa, M. Rossi, A. Saura-Ródenas and F. L. Martínez-Viviente are with the Department of Electronics and Computer Technology, Technical University of Cartagena. E-30202 Cartagena, Spain (e-mail: juan.hinojosa@ upct.es).

A. Álvarez Melcón is with the Information and Communications Technology Department, Technical University of Cartagena. E-30202 Cartagena, Spain.

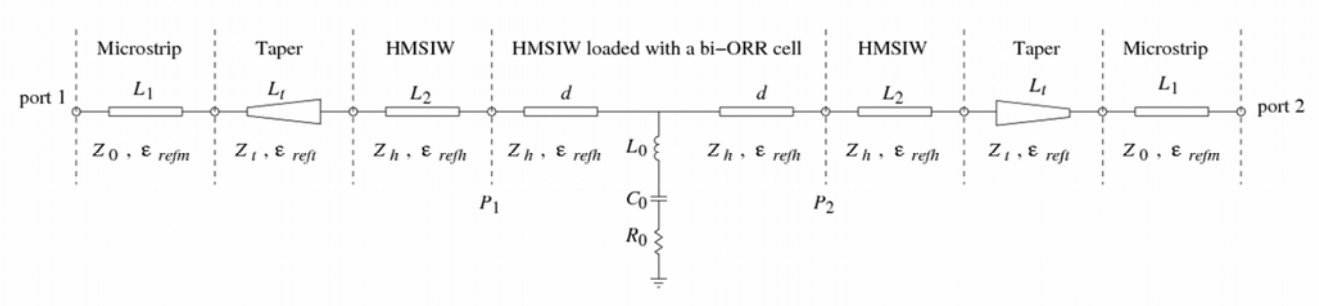

Fig. 2. Simplified equivalent circuit model of the HMSIW structure loaded with a BC-OSRR cell.

During the last years there has been a great interest in the design of microwave filters in SIW technology based on metamaterial-inspired structures, due to their attractive features to reduce the size of the circuits. The proposed SIW structures implement band-pass and band-stop filters. They are mainly implemented by means of defected ground structures (DGS) [11], [12], electromagnetic bandgap (EBG) patterns [13]-[15] or different versions of split ring resonators (SRR) [16]-[20]. EBGs are obtained by means of periodic patterns, while DGSs are based on a single defect or several defects realized on the ground plane of circuits. The SRR versions have two split rings of different radii. The design of filters by means of DGSs and SRRs are easier than EBGs, since they behave as *LC* resonators and, therefore, it is simpler to extract their equivalent circuits. EBG-based SIW filters require a larger size than DGS- and SRR-based SIW filters, due to their periodic patterns. The SRR-based SIW filters have two interesting features with respect to the EBG and DGS structures. On the one hand, their electrical characteristics are easily controllable through their geometric parameters (radius, width of the ring, etc.) and on the other hand their electric sizes are more compact. In the previous works that use SRR-based SIW filters, only complementary split ring resonator (CSRR) [21], [22] and open complementary split ring resonator (OCSRR) cells [23], [24] have been applied, due to the difficulty of inserting an open version of the split ring resonator (OSRR) such as that of [25] in a SIW line. Unlike SRRs and CSRRs which are coupled to a circuit, the open configurations have input and output ports allowing a series or parallel connection with a circuit and, therefore, a better excitation of the resonator. Recently, a solution was proposed for the design of band-stop filters by embedding an open ring resonator (ORR) within a HMSIW structure [26], [27]. However, the equivalent circuit model of this ORR cell includes a connection to ground by means of a radiation resistance at the resonant frequency, which models undesired radiation effects that deteriorate band-stop filter performance.

In this paper, we propose to minimize this drawback by inserting a new version of the open interconnected split ring resonator (OISRR) [28]-[30] within a HMSIW structure. This new cell, named broadside coupled open split ring resonator (BC-OSRR), consists of two overlapping rings separated by a substrate instead of two rings in the same plane as for the OISRR cell. This BC-OSRR cell is connected in parallel with a section of HMSIW. This combination allows implementing a compact design of band-stop HMSIW filters. In comparison with the OISRR and ORR cells, the BC-OSRR cell has the ability of minimizing radiation loss, increasing the compactness and improving the stop-band rejection level. The description, equivalent circuit and analysis of the HMSIW loaded with a BC-OSRR cell are presented in Section II. Emphasis has been placed on radiation effects and radiation resistances of HMSIW structures loaded with the proposed cell and other resonators (ORR, OISRR) [26], [28]. An experimental validation by means of a band-stop HMSIW prototype loaded with a BC-OSRR is provided in Section III. The results are compared with other high-performance band-stop filters using different technologies (microstrip, CPW, SIW) and resonators (open-stub, SRR, CSRR, OSRR, ORR, OISRR) [19], [20], [24], [26]-[29], [31]-[40]. Measured results of a second-order BC-OSRR-based HMSIW band-stop filter are also discussed. Finally, conclusions are presented in Section IV.

II. Band-Stop HMSIW Filter using a BC-OSRR

A. Structure and Equivalent Circuit Model

The structure and equivalent circuit model of the proposed band-stop HMSIW filter loaded with the BC-OSRR cell are shown in Figs. 1 and 2, respectively. The BC-OSRR cell is a modified version of the open interconnected split ring resonator (OISRR) [28], [29]. Unlike the OISRR cell which has two rings in the same plane, the new BC-OSRR cell is designed by means of two broadside coupled rings separated by a substrate and connected to a planar waveguide, thus minimizing the problem of radiation loss and increasing the compactness and the stop-band rejection level. In Fig. 1(a), corresponding to the top side of the structure, the dimensions of the BC-OSRR cell are the external radius *r*, width *c* of the ring conductor strip and gap *g*. At the bottom side, a window $D_1 \times D_2$ without metal is opened and a ring with the same dimensions as the one at the top side is printed. The top ring and bottom ring are separated by a substrate thickness *h* of relative permittivity ε_r. Both rings are aligned with each other. The gaps *g* of the top and bottom rings are etched in opposite directions. As it can be seen, both rings (Fig. 1(c)) are connected to a common point of a HMSIW section. A microstrip to HMSIW transition has been implemented in both ports of the structure to carry out measurements. This transition consists of a tapering microstrip section of length L_t with two different widths (W_m, W_t). It connects the microstrip line of length L_1 and impedance Z_0

with the HMSIW section of length L_2 and impedance Z_h. This transition allows to transform the quasi-TEM mode of the microstrip line (W_m) into the TE$_{10}$ mode of the HMSIW (W_{HMSIW}). Thus, the BC-OSRR cell is connected to ports 1 and 2 by means of two microstrip lines, two microstrip to HMSIW transitions and two HMSIW sections of lengths L_1, L_t and L_2, respectively. In this work, the size of the ground plane covers the width of the HMSIW and surrounds the open window to reduce processing time during the fabrication of the structures by means of a milling machine. The ground plane can be reduced to the width W_{HMSIW} of the HMSIW (except for the frame of the window). It can also be reduced in the areas below the microstrip lines and microstrip to HMSIW transitions. Note that these modifications can lead to slight differences with respect to the results presented in this manuscript. In particular, the close proximity of the finite ground plane to the microstrip line can slightly affect the characteristic impedance of the port, resulting in a degradation of the return losses. However, this can be compensated by adjusting the width of the microstrip line to recover the right value of the port impedance.

A simplified equivalent circuit (Fig. 2) of the HMSIW structure loaded with the BC-OSRR cell was determined from electromagnetic (EM) analysis of its frequency response. It consists of a series R_0 L_0 C_0 resonant circuit shunted between two loaded HMSIW sections. Each loaded HMSIW section has a length $d = D_1/2$. Unlike the OISRR and ORR cells [26]-[30] that are connected to ground by means of a radiation and ohmic resistance, the BC-OSRR cell is linked to ground only through an ohmic resistance, minimizing radiation loss and improving stop-band rejection level. From the equivalent circuit model of the BC-OSRR, a resonant frequency f_0 leading to a transmission zero can be identified. This frequency is obtained from the shunt series circuit $f_0 = 1/(2\pi\sqrt{L_0C_0})$, which has a reactance slope $s_0 = 2\pi f_0 L_0$. The elements R_0, L_0 and C_0 of the equivalent circuit depend on the design parameters (r, c, g, h, ε_r) of the BC-OSRR cell. Their values can be derived by means of the simulations or measurements of the transmission parameter S_{21}. Considering the two-port network equivalent circuit (Fig. 2) without the microstrip lines and without the tapering microstrip sections of respective lengths L_1 y L_t, the two ports terminated with the characteristic impedance of the HMSIW Z_h for the dominant propagating TE$_{10}$ mode [41], and the shunt branch $Z = j\omega L_0 + 1/(j\omega C_0)$, then the transmission parameter S_{21} can be defined by

$$S_{21} = \frac{1}{1+Z_h/(2Z)} \quad (1)$$

The L_0 and C_0 elements can be determined by means of equation (1) and the 3 dB stop-band bandwidth Δf_0. Assuming that $f = f_0 + \Delta f_0/2$ and the narrow band approximations [1], $\Delta f_0 << f_0$ and $(f/f_0 - f_0/f) \approx 2\Delta f_0/f_0$, then the shunt impedance can be approximated by $Z \approx j2\pi f_0 L_0(2\Delta f_0/f_0)$.

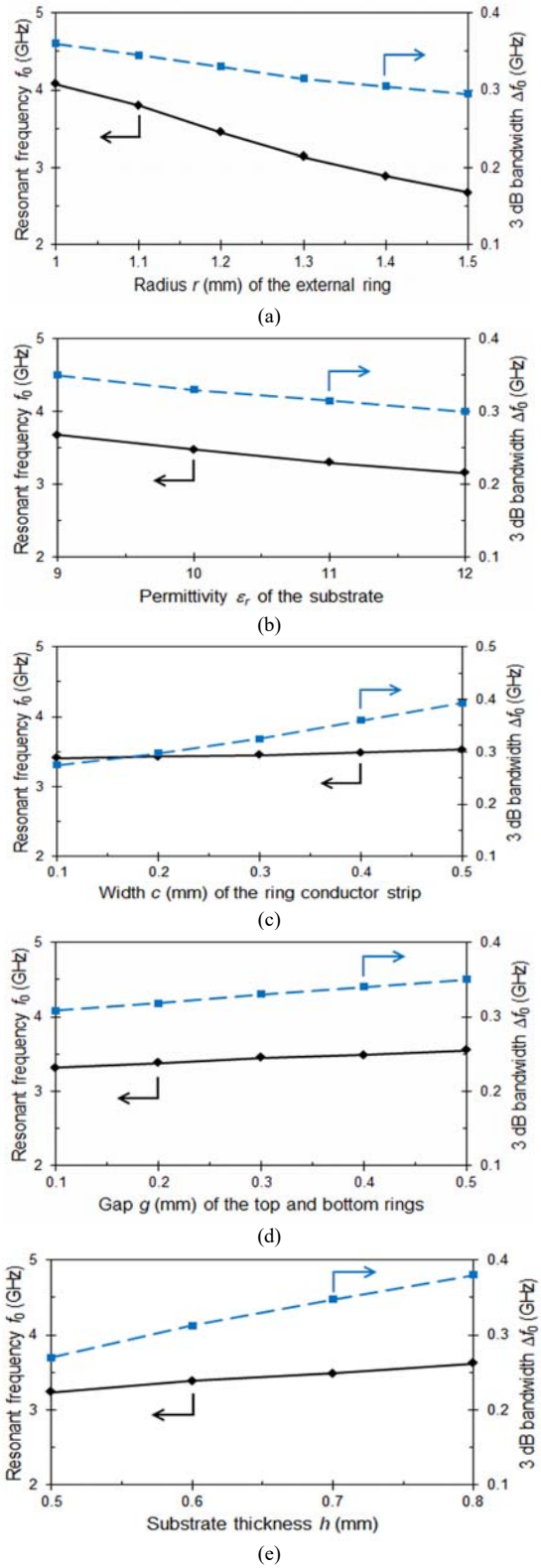

Fig. 3. Resonant frequency f_0 and 3 dB stop-band bandwidth Δf_0 for the HMSIW loaded with a BC-OSRR cell as a function of design parameters (dimensions in mm). (a) r (c = g = 0.3, h = 0.635 and ε_r = 10.2 fixed). (b) ε_r (r =1.2, c = g = 0.3 and h = 0.635 fixed). (c) c (r = 1.2, g = 0.3, h = 0.635 and ε_r = 10.2 fixed). (d) g (r = 1.2, c = 0.3, h = 0.635 and ε_r = 10.2 fixed). (e) h (r =1.2, c = g = 0.3 and ε_r = 10.2 fixed).

Substituting it in (1) and taken into account the modulus of $|S_{21}|$ = 0.707 at the cut-off frequency, then Δf_0 can be derived as

$$\Delta f_0 = Z_h \frac{f_0}{2s_0} \tag{2}$$

and thus the L_0 and C_0 elements can be calculated

$$L_0 = \frac{Z_h}{4\pi\Delta f_0} \tag{3}$$

$$C_0 = \frac{1}{L_0}(2\pi\ f_0)^{-2} \tag{4}$$

Finally, the unloaded quality factor Q_u and the return loss $|S_{11}|$ measured at the resonant frequency f_0 allow to obtain the resistance R_0

$$Q_u = \frac{f_0}{\Delta f_0\left(1-|S_{11}|_{f0}\right)} \tag{5}$$

$$R_0 = \frac{2\pi\ f_0\ L_0}{Q_u} \tag{6}$$

B. Analysis and Design of the HMSIW Structure Loaded with a BC-OSRR Cell

Figs. 3 and 4 illustrates, respectively, the effects of the design parameters (r, c, g, h, ε_r) of the BC-OSRR cell for the HMSIW on the resonant frequency f_0 and the 3 dB stop-band bandwidth Δf_0, and on the inductance L_0 and capacitance C_0 of the ring resonator. The results presented in Fig. 3 were obtained by means of a commercial full-wave 3D electromagnetic (EM) simulator (ANSYS HFSS), while those in Fig. 4 were achieved using equations (1) to (6) to link equivalent circuit lumped element values with the EM data. The variation of the resistance R_0 has not been included in Fig. 4. Its value is between 0.28 Ω and 0.66 Ω. We have been able to observe that a decrease of the resonant frequency f_0 contributes to a reduction of the resistance R_0, while an increase of the resonant frequency f_0 promotes a rise of the resistance R_0. In Fig. 3(a), it can be seen that the resonant frequency f_0 (solid line) and the 3 dB bandwidth of the stop-band Δf_0 (dashed line) decrease as the radius r of the external ring increases from 1 mm to 1.5 mm ($c = g = 0.3$ mm, $h = 0.635$ mm and $\varepsilon_r = 10.2$ are constant). Larger radius r contributes to an increase of the inductance L_0 and capacitance C_0 as it can be seen in Fig. 4(a). A similar behavior is observed in Fig. 3(b) when the relative permittivity ε_r of the substrate increases from 9 to 12. In this case, the design parameters r =1.2 mm, $c = g$ = 0.3 mm and h = 0.635 mm are constant and, therefore, C_0 (Fig. 4(b)) increases with increasing relative permittivity ε_r. At the

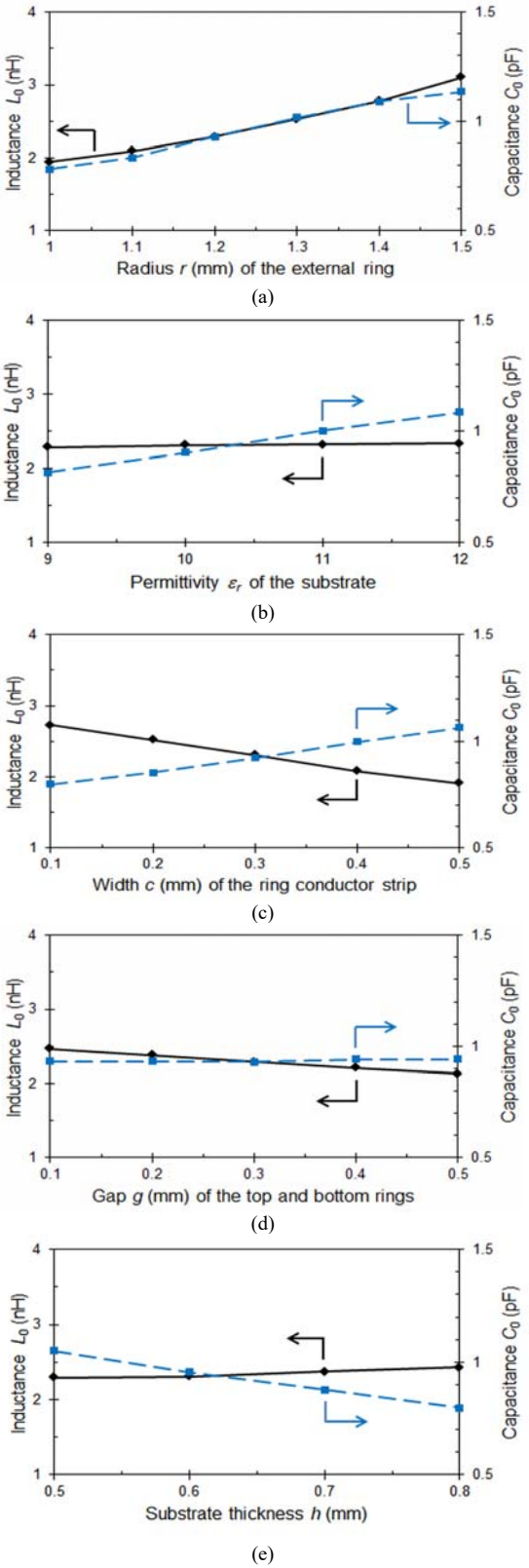

Fig. 4. Inductance L_0 and capacitance C_0 for the HMSIW loaded with a BC-OSRR cell as a function of design parameters (dimensions in mm). (a) r (c = g = 0.3, h = 0.635 and ε_r = 10.2 fixed). (b) ε_r (r =1.2, $c = g$ = 0.3 and h = 0.635 fixed). (c) c (r = 1.2, g = 0.3, h = 0.635 and ε_r = 10.2 fixed). (d) g (r = 1.2, c = 0.3, h = 0.635 and ε_r = 10.2 fixed). (e) h (r =1.2, $c = g$ = 0.3, and ε_r = 10.2 fixed).

same time, L_0 (Fig. 4(b)) is constant with increasing relative permittivity ε_r of the substrate and, therefore, the resonant frequency f_0 and the 3 dB stop-band bandwidth decrease. Fig. 3(c) shows an opposite trend of the 3 dB stop-band bandwidth Δf_0 as compared to the previous ones, when the width c of the ring conductor strip increases from 0.1 to 0.5 (r = 1.2, g = 0.3, h = 0.635 and ε_r = 10.2 are constant). The capacitance C_0 (Fig. 4(c)) increases with increasing width c of the ring conductor strip, while the inductance L_0 (Fig. 4(c)) decreases, which leads to an enlarged 3 dB stop-band bandwidth. The width c of the ring conductor strip has little influence on the resonant frequency f_0, since this frequency is quasi-constant for values of c between 0.1 and 0.5. This is because the decrease of the inductance L_0 is compensated by the increase of the capacitance C_0. In Figs. 3(d) and 3(e), it can be seen that the gap g (r = 1.2, c = 0.3, h = 0.635 and ε_r = 10.2 constant) and the substrate thickness h (r =1.2, c = g = 0.3, and ε_r = 10.2 fixed) have the same influence on the resonant frequency f_0 and the 3 dB stop-band bandwidth Δf_0. The resonant frequency f_0 and the 3 dB stop-band bandwidth Δf_0 increase as the gap g and the substrate thickness h rise, respectively, from 0.1 to 0.5 and 0.5 to 0.8. The inductance L_0 decreases slightly (Figs. 4(d)) or increases slightly (Fig. 4(e)), because the other design parameters r = 1.2, c = 0.3 and ε_r = 10.2 are constant. Finally, the capacitance C_0 is quasi-constant as the gap g increases (Fig. 4(d)) and decreases as the substrate thickness h (Fig. 4(e)) increases, which lead to an increase in the resonant frequency f_0 and the 3 dB stop-band bandwidth Δf_0.

An efficient empirical model of the BC-OSRR cell based on a linear regression approach [42] was generated by means of data obtained from Figs. 3 and 4. Thus, it is possible to have the geometric parameters of the BC-OSRR cell as a function of the resonant frequency f_0 and the 3 dB bandwidth Δf_0, and also the values of R_0, L_0 and C_0. Then, the dimensions of the HMSIW, tapering microstrip section, microstrip line and BC-OSRR cell were optimized by means of [9], [43], [44] and this empirical model to ensure a resonant frequency at f_0 = 3.5 GHz and a 3 dB stop-band bandwidth of Δf_0 = 0.4 GHz. Fig. 5 shows the frequency responses of the HMSIW structure loaded with a BC-OSRR cell by means of EM and circuit simulations. The dimensions and the relative permittivity of the substrate are included in the caption of Fig. 5. The element values used in the equivalent circuit of the BC-OSRR cell are: R_0 = 0.4 Ω, L_0 = 2.28 nH and C_0 = 0.93 pF. The frequency responses (Fig. 5) were obtained with commercial simulators (Ansys HFSS and Keysight ADS). The circuit ADS simulator allows simulating the equivalent circuit represented in Fig. 2, including the half-mode substrate integrated waveguides (HMSIWs) filled with a substrate ε_r by using the RWG (rectangular waveguide) model. The width of the RWGs was 2 times W_{HMSIW} and the metallic cylinder rows of the HMSIWs were considered as electric walls

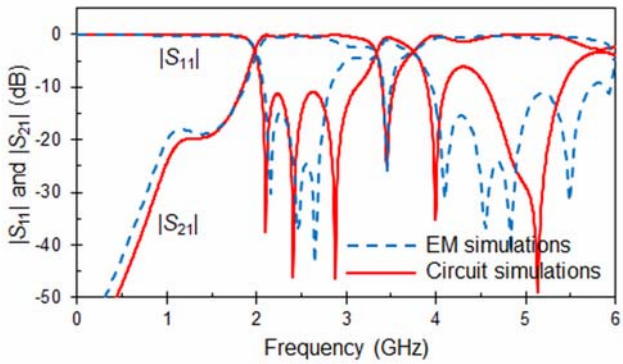

Fig. 5. Comparison of EM and circuit frequency responses for the HMSIW loaded with a BC-OSRR cell (dimension in mm): W_{HMSIW} = 11.65, s = 1.2, d = 0.6, Wm = 0.594, W_t = 4.66, L_t = 28.95, L_1 = 5, L_2 = 12.45, r = 1.21, c = 0.3, g = 0.3, $D_1 \times D_2$ = 5.1 × 5.1, h = 0.635, ε_r = 10.2.

of perfect conductor. A copper thickness of t = 0.017 mm was taken into account in the EM and circuit simulations. In Fig. 5, it can be seen two characteristics for the EM simulations (dashed lines). The first one is inherent to the HMSIW, which presents a frequency response of high-pass type with a cut-off frequency defined at f_c = 2 GHz. The second characteristic is relative to the transmission zero which appears in the pass-band of the HMSIW. This is a consequence of the resonance of the BC-OSRR cell at f_0 = 3.45 GHz, since an electric short to ground occurs and the incident signal is reflected back to the input port. Return and insertion loss at f_0 = 3.45 GHz are, respectively, 1 dB and 26.1 dB, while 3 dB stop-band bandwidth is Δf_0 = 0.4 GHz (11.5%). The previous data and (5) give an unloaded quality factor of Q_u = 79. In Fig. 5, it can be seen that the results (solid lines) obtained by means of the equivalent circuit shown in Fig. 2 with the previous R_0, L_0 and C_0 data also present a high-pass characteristic with a stop-band rejection in its pass-band. The resonance of the BC-OSRR appears at f_0 = 3.5 GHz and the 3 dB stop-band bandwidth is Δf_0 = 0.4 GHz. Both agree well with the values obtained from EM simulations. The differences in the pass-bands are due to the simplicity of the circuit model employed, that does not consider the interactions and coupling between the different discontinuities and transitions present in the physical structure. However, in practical designs the circuit may be useful to obtain an initial structure, for a subsequent optimization process.

To check that the BC-OSRR cell works as a band-stop filter we have analyzed the behavior of the HMSIW loaded with a BC-OSRR cell by studying the electric and magnetic field distribution (Fig. 6) within its structure at three different frequencies. One is below the cut-off frequency of the HMSIW (f_1 = 0.5 GHz) and the other two are inside its pass-band (f_2 = 3.45 GHz and f_3 = 4.5 GHz). In Fig. 6(a), it can be seen that

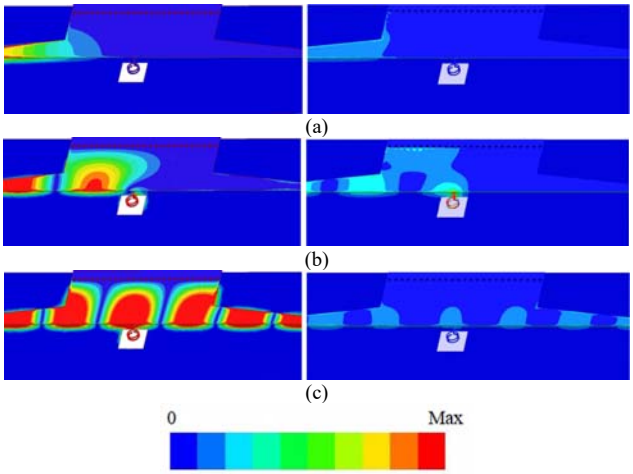

Fig. 6. Magnitude of the electric (left) and magnetic (right) field distribution within the HMSIW structure loaded with a BC-OSRR cell for the TE10 mode at four different frequencies. (a) f_1 = 0.5 GHz. (b) f_2 = 3.45 GHz. (c) f_3 = 4.5 GHz. The maximum value (Max) of the colorbar is 5000 V/m for the electric field and 500 A/m for the magnetic field. The incident power is 1 W.

the BC-OSRR cell does not resonate at $f_1 = 0.5$ GHz, and the signal is not transmitted to the output port. This is because the signal has a frequency lower than the cut-off frequency of the HMSIW. At $f_2 = 3.45$ GHz (Fig. 6(b)), we are in the pass-band of the HMSIW. However, the electric and magnetic fields of the BC-OSRR cell resonate strongly and this eliminates any transmission between the input and output ports. Finally, Fig. 6(c) depicts the electric and magnetic fields at $f_3 = 4.5$ GHz, corresponding to the pass-band of the HMSIW, far from the notch frequency. The BC-OSRR cell does not resonate and the signal is transmitted to the output port. The field distribution essentially displays the TE_{10} mode in the HMSIW structure loaded with a BC-OSRR cell. Specially, this can be observed in the plot of the magnetic field, which shows very small currents induced on the ring structure.

C. Radiation Effects

The HMSIW structure loaded with the BC-OSRR can experience radiation effects due to the open window $D_1 \times D_2$ at the bottom side. Thus, we have analyzed the forward loss factor F_{LF} (Fig. 7) of the structure by means of EM simulations as a function of frequency and different sizes of the open window

$$F_{LF} = 1 - |S_{11}|^2 - |S_{21}|^2 \quad (7)$$

To take into consideration only the radiation effects, we have considered perfect conductors and a lossless substrate in the EM simulations. The dimensions of the HMSIW structure loaded with the BC-OSRR and the relative permittivity of the substrate are included in the caption of Fig. 7. They are the same as those used for the HMSIW structure loaded with the BC-OSRR in the EM simulations shown in Fig. 5. As it can be seen in Fig. 7, radiation losses present three peaks in the frequency range 0 – 6 GHz. The first peak appears at the cut-off frequency (f_c = 2 GHz) of the HMSIW, the second is located at the resonant

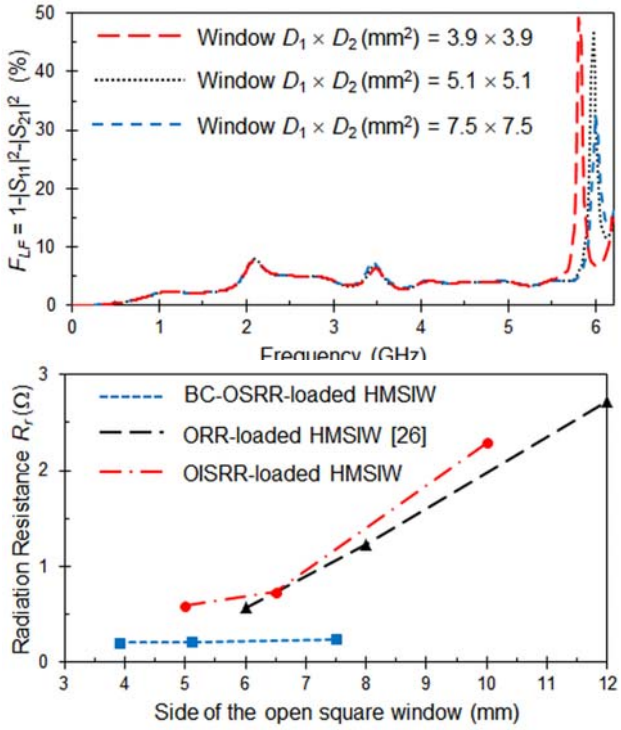

Fig. 8. Radiation resistance at the resonant frequency f_0 = 3.5 GHz as a function of the size of the open square window for HMSIWs loaded with BC-OSRR, ORR and OISRR cells. They were optimized to have a resonant frequency at f_0 = 3.5 GHz. Dimension (mm): W_{HMSIW} = 11.65, s = 1.2, d = 0.6, W_m = 0.594, W_t = 4.66, L_t = 28.95, L_1 = 5, L_2 = 12.45, h = 0.635, ε_r = 10.2. r = 1.21, c = 0.3, g = 0.3 for the BC-OSRR. r = 1.9, c = 0.3, g = 0.3 for the ORR. r = 1.55, c = 0.3, s = 0.25, g = 0.3 for the OISRR.

frequency of the BC-OSRR (f_0 = 3.5 GHz) and the last one is around 6 GHz, which corresponds to a spurious resonance (f_s). Unlike OISRR and ORR cells [26]-[30], the different sizes of the open window have little effect on radiation losses of the BC-OSRR cell for the first two peaks, which are lower than 8%. This can be verified in Fig. 8, which represents the radiation resistance at the resonant frequency f_0 = 3.5 GHz as a function of the size of the open square window for HMSIWs loaded with BC-OSRR, ORR and OISRR cells. The ORR and OISRR cells with the dimensions included in the caption of Fig. 8 were optimized to have a resonant frequency at f_0 =3.5 GHz in the same way as for the BC-OSRR cell. In Fig. 8, the radiation resistance of the band-stop HMSIW filter loaded with the BC-OSRR cell is around 0.2 Ω and almost constant as a function of the size of the open window, while the filters using ORR and OISRR cells have a minimum radiation resistance around 0.6 Ω, which increases with the size of the open window. In Fig. 7, the radiation loss at the spurious resonance can be reduced by increasing the size of the open window to $D_1 \times D_2$ (mm²) = 7.5 × 7.5, at the expense of increasing the size of the structure. The smallest open window option $D_1 \times D_2$ (mm²) = 3.9 × 3.9

TABLE I
COMPARISON BETWEEN THE PROPOSED HMSIW BAND-STOP FILTER LOADED WITH A BC-OSRR AND OTHER BAND-STOP FILTERS USING DIFFERENT TECHNOLOGIES AND RESONATORS

Technology	Resonators	references	f_0 (GHz)	3 dB FBW (%)	*IL* (dB)	*RL* (dB)	2-D size ($\lambda_0 \times \lambda_0$)
Microstrip	Open-stub	[31] Fig. 2	4.5	52.8	45	-	0.27×0.12
CPW	Open-stub	[32] Fig. 6	24.5	92	30	0.5	0.016×0.18
HMSIW	Open-stub	[33] Fig. 5	14.7	24	36	-	0.106×0.03
Microstrip	CSRR	[34] Fig. 3(b)	2.5	24	60	-	0.233×0.025
Microstrip	CSRR	[35] Fig. 6	2	30	28	-	0.066×0.042
CPW	CSRR	[36] Fig. 6	3.5	15.7	40	-	0.59×0.042
CPW	CSRR	[37] Fig. 4	7.7	5.2	25	2.5	0.307×0.107
CPW	CSRR	[38] Fig. 5	5.8	6	11.5	-	0.07×0.07
SIW	CSRR	[19] Fig. 3(c)	31	11.3	45	1	0.375×0.6
Microstrip	SRR	[36] Fig. 3	4.5	22.2	30	-	1.28×0.068
Microstrip	SRR	[39] Fig. 2	9.25	5.4	40	5	0.609×0.242
Microstrip	SRR	[39] Fig. 5	9.25	1.5	10	-	0.032×0.242
CPW	SRR	[36] Fig. 2	6.5	12.3	18	-	0.87×0.217
CPW	SR	[40] Fig. 3	3.5	11.4	20	2.1	0.169×0.182
SIW	SRR	[20] Fig. 21	4.39	20.5	30	-	0.625×0.014
CPW	OSRR	[24] Fig. 4	5.5	37	65	-	0.27×0.17
Microstrip	ORR	[30] Fig. 4	3.7	9.7	16.3	1.9	0.111×0.111
CPW	ORR	[27] Fig. 7	3.46	20.2	21	0.9	0.105×0.105
HMSIW	ORR	[26] Fig. 2	3.5	4.6	16	2.7	0.094×0.094
Microstrip	OISRR	[28] Fig. 6(a)	2.2	1.5	12.6	3.6	0.066×0.066
CPW	OISRR	[29] Fig. 5	2.2	4	11.7	2.9	0.066×0.066
HMSIW	BC-OSRR	This work Fig. 11	3.5	9.2	21.6	1.3	0.059×0.059

f_0 is the resonant frequency, 3 dB FBW is the fractional bandwidth at 3 dB, *IL* and *RL* are, respectively, insertion and return losses at f_0, and λ_0 is the free-space wavelength at f_0.

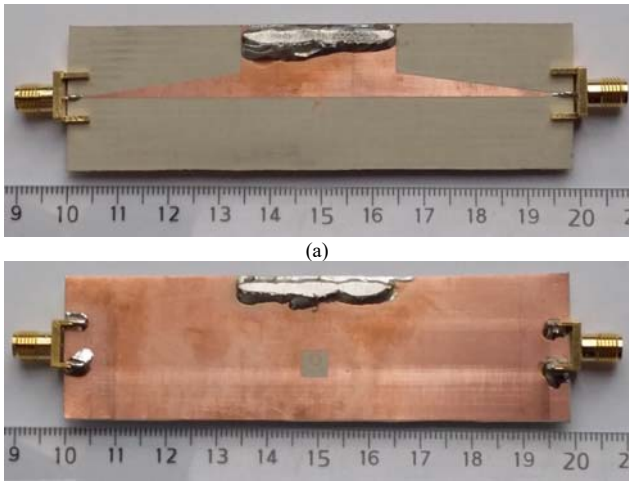

(a)

(b)

Fig. 9. Photographs of the fabricated HMSIW structure loaded with a BC-OSRR cell. (a) Top side. (b) Bottom side. Dimension (mm): W_{HMSIW} = 11.65, s = 1.2, d = 0.6, W_m = 0.594, W_t = 4.66, L_t = 28.95, L_1 = 5, L_2 = 12.45, r = 1.21, c = 0.3, g = 0.3, $D_1 \times D_2$ = 5.1 × 5.1, h = 0.635, ε_r = 10.2.

causes the spurious resonance being shifted downwards by 0.2 GHz and the radiation loss increasing up to 45.2%. Accordingly, as a compromise, the design of the proposed band-stop HMSIW filter was made with the intermediate open window $D_1 \times D_2$ (mm^2) = 5.1 × 5.1.

III. RESULTS

An interesting application of the proposed BC-OSRR cell is the design of band-stop filters. As illustrative examples, first- and second-order band-stop HMSIW filters were designed and fabricated (Figs. 9 and 10) by means of a milling machine on a RT/Duroid 6010 substrate with the following characteristics

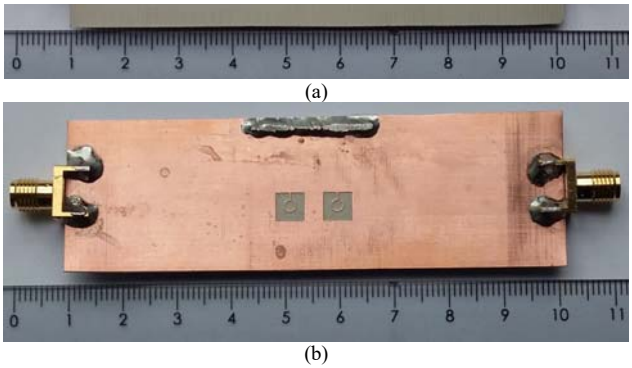

(a)

(b)

Fig. 10. Photographs of the fabricated second-order band-stop HMSIW filter loaded with two BC-OSRR cells. (a) Top side. (b) Bottom side. Dimension (mm): W_{HMSIW} = 11.65, s = 1.2, d = 0.6, W_m = 0.594, W_t = 4.66, L_t = 28.95, L_1 = 5, L_2 = 4.25, r = 1.21, c = 0.3, g = 0.3, $D_1 \times D_2$ = 5.1 × 5.1, h = 0.635, ε_r = 10.2.

and dimensions: ε_r = 10.2, tgδ = 0.0023 at 10 GHz, copper thickness t = 0.017 mm and substrate thickness h = 0.635 mm. The measurements were carried out by means of a vector network analyzer (VNA, R&S ZVA 67 GHz) between 0.01 GHz and 6 GHz. A previous calibration was performed by means of an automatic calibration unit (R&S Zv-Z52) at the outputs of the two coaxial cables connected to the VNA. The two reference planes of the measurements are at the two outputs of the coaxial cables. Two coaxial (SMA) to microstrip adapters were soldered (Figs. 9 and 10) to each band-stop HMSIW filter to carry out measurements.

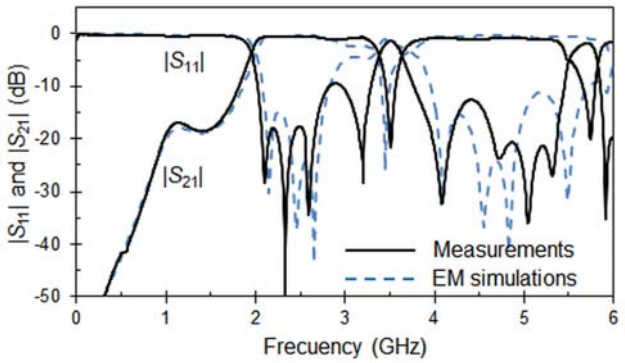

Fig. 11. EM simulation and measured frequency responses of the prototyped first-order band-stop HMSIW filter loaded with a BC-OSRR cell shown in Fig. 9.

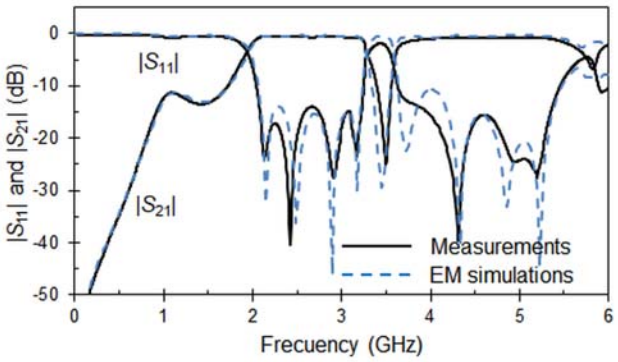

Fig. 12. EM simulation and measured frequency responses of the prototyped BC-OSRR-loaded second-order band-stop HMSIW filter loaded with two BC-OSRR cells shown in Fig. 10.

The dimensions of the first-order band-stop prototype are the same as those used for the HMSIW structure loaded with a BC-OSRR cell in the EM simulations shown in Fig. 5. They were obtained for a resonant frequency of f_0 = 3.5 GHz with a 3 dB stop-band bandwidth of Δf_0 = 0.4 GHz. The second-order band-stop filter is based on two cascaded BC-OSRR cells, separated by a quarter wavelength HMSIW section acting as impedance inverter (λ_g = 33.88 mm for f_0 = 3.5 GHz and ε_{ref} = 6.4). The slope parameters of the BC-OSRR cells were scaled to keep the same characteristic impedance in all HMSIW sections.

EM and measurement frequency responses of the first-order band-stop prototype (Fig. 9) loaded with the BC-OSRR cell are represented in Fig. 11. As it can be seen, EM simulations and measurement results differ slightly. This is due to the SMA adapters, which were not considered in the calibration procedure, and also to the fabrication tolerances. However, both responses present similar characteristics. The measurements (Fig. 11) show a typical high-pass behavior of the HMSIW with a cut-off frequency at f_c = 1.98 GHz. Moreover, in the passband of the HMSIW, there is a transmission zero at the resonant frequency f_0 = 3.5 GHz of the BC-OSRR cell. At this frequency, an electric short to ground occurs and, therefore, the incident power is reflected back to the input source as in Fig. 6(b). The HMSIW structure loaded with the BC-OSRR cell works as a band-stop filter at the frequency f_0 = 3.5 GHz. Return and insertion losses at f_0 = 3.5 GHz are 1.3 dB and 21.6 dB, respectively. The 3 dB stop-band bandwidth and unloaded quality factor are, respectively, Δf_0 = 0.32 GHz (9.2%) and Q_u = 79. The passbands of the band-stop filter are shaped with a reflection zero close to the stopband introduced by the BC-OSRR. Also, it can be observed additional reflection zeros in the passbands. These additional reflection zeros are produced by the matching level achieved by the microstrip to HMSIW transitions, which in our design leads to return losses better than 10 dB. In addition, in the lower passband we can clearly observe the effect of the cut-off frequency of the TE_{10} mode in the HMSIW structure. The electrical length of the BC-OSRR cell for D_1 = 5.1 mm is lower than $\lambda_g/6$ (λ_g = 33.88 mm for f_0 = 3.5 GHz and ε_{ref} = 6.4). This confirms the reduced size of the proposed BC-OSRR cell with respect to a conventional $\lambda/2$ resonator.

Table I provides a comparison between the proposed first-order band-stop HMSIW filter and several previous works using microstrip, CPW and SIW technologies loaded with different resonators (open-stub, SRR, CSRR, OSRR, ORR, OISRR) [19], [20], [24], [26]-[29], [31]-[40]. In some manuscripts, return loss (*RL*) is not provided. The SRR and CSRR resonators are coupled to a CPW, microstrip or SIW line, while the different open ring resonators (OSRR, OISRR, ORR, bi-ORR or BC-OSRR) and the open stubs have a parallel connection with a CPW, microstrip or SIW line. This allows a better excitation of the resonator and control of the resonant frequency. As it can be seen in Table I, the 3 dB fractional bandwidth (FBW) varies between 24% and 52.8% for the band-stop filters loaded with stubs, 5.2% and 30% for CSRRs, 1.5% and 22.5% for SRRs and 1.5% and 37% for open-SRRs. Insertion loss (*IL*) also varies according to the cell used and it depends on the number of cascaded cells. In terms of size, the microstrip, CPW and SIW band-stop filters loaded with any of the resonators have a larger size than the proposed band-stop HMSIW filter loaded with a BC-OSRR cell. Compared with the recent OISRR and ORR cells [26]-[30], the BC-OSRR cell has a larger 3 dB FBW, better insertion (*IL*) and return (*RL*) losses, except for the CPW structure loaded with a ORR cell [27], which has lower *RL*. However, when the ORR cell is connected to a HMSIW [26], *RL* deteriorates, increasing from 0.9 dB to 2.7 dB. Note that some of these characteristics achieved with the new BC-OSRR are superior to those reported in these previous publications. The 2-D size of the BC-OSRR cell is $0.059\lambda_0 \times 0.059\lambda_0$, while the OISRR cell has a 2-D size of $0.066\lambda_0 \times 0.066\lambda_0$. The 2-D size of the band-stop HMSIW loaded with the ORR cell [26] is even larger: $0.094\lambda_0 \times 0.094\lambda_0$.

Fig. 12 shows EM and measured *S*-parameters for the second-order band-stop HMSIW filter. In the same way as for the first-order filter, EM simulations and measurement results differ slightly, due to the SMA adapters which were not taken into account in the calibration procedure, and also to the fabrication tolerances. However, both responses exhibit similar characteristics. They have a high-pass characteristic with a cut-

off frequency at f_c = 1.95 GHz and a rejection band in the pass-band of the HMSIW. In Fig. 12, the center frequency of the band-stop is f_0 = 3.5 GHz, while the 3 dB stop-band bandwidth is Δf_0 = 0.35 GHz (10%). The return and insertion losses at f_0 = 3.5 GHz are 1.9 dB and 25 dB, respectively.

IV. Conclusion

A compact band-stop half-mode substrate integrated waveguide (HMSIW) filter using a broadside coupled open split ring resonator (BC-OSRR) is proposed in this paper for the first time. The BC-OSRR cell is conceived by two rings with the same dimensions and aligned with each other on opposite sides of the substrate. This BC-OSRR cell is connected in parallel to a common point of a HMSIW section by etching an open window in the metallized bottom side. The electromagnetic analysis of the structure has allowed us to derive a simple equivalent circuit model and to show two main characteristics. The HMSIW structure loaded with an appropriate BC-OSRR cell has a high-pass behavior with a stop-band rejection in its pass-band. Low undesired radiation loss has been observed in the working frequency range. Good performance has been obtained from fabricated prototypes of first- and second-order band-stop HMSIW filters. The BC-OSRR cell integrated within a HMSIW can be useful for the future development of new applications requiring band rejection filters.

References

[1] J. S. Hong and M. J. Lancaster, *Microstrip filters for RF/microwave applications*. New York, NY, USA: Wiley, 2001.

[2] H. Uchimura, T. Takenoshita, and M. Fujii, "Development of a laminated waveguide," *IEEE Trans. Microw. Theory Techn.*, vol. 46, no. 12, pp. 2438-2443, Dec. 1998.

[3] D. Deslandes and K. Wu, "Integrated microstrip and rectangular waveguide in planar form," *IEEE Microw. Compon. Lett.*, vol. 11, no. 2, pp. 68-70, Feb. 2001. doi: 10.1109/7260.914305.

[4] Y. Cassivi, L. Perregrini, P. Arcioni, B. Bressan, K. Wu, and G. Gonciauro, "Dispersion characteristics of substrate integrated rectangular waveguide," *IEEE Microw. Compon. Lett.*, vol. 12, no. 9, pp. 333-335, Sep. 2002. doi: 10.1109/LMWC.2002.803188.

[5] D. Deslandes and K. Wu, "Single-substrate integration technique of planar circuits and waveguide filters," *IEEE Trans. Microw. Theory Techn.*, vol. 51, no. 2, pp. 593-596, Feb. 2003.

[6] F. Xu and K. Wu, "Guided-wave and leakage characteristics of substrate integrated waveguide," *IEEE Trans. Microw. Theory Techn.*, vol. 53, no. 1, pp. 66-73, Jan. 2005. doi: 10.1109/TMTT.2004.839303.

[7] D. Deslandes and K. Wu, "Accurate modeling, wave mechanism, and design considerations of a substrate integrated waveguide," *IEEE Trans. Microw. Theory Techn.*, vol. 54, no. 6, pp. 2516-2526, Jun. 2006. doi: 10.1109/TMTT.2006.875807.

[8] W. Hong *et al.*, "Half mode substrate integrated waveguide: A new guided wave structure for microwave and millimeter wave applications," in *Proc. Joint 31st Int. Infrared Millimeter Wave Conf./14th Int. Terahertz Electron. Conf.*, 2006, pp. 18-22.

[9] Q. Lai, C. Fumeaux, W. Hong, and R. Vahldieck, "Characterization of the propagation properties of the half-mode substrate integrated waveguide," *IEEE Trans. Microw. Theory Techn.*, vol. 57, no. 8, pp. 1996-2004, Aug. 2009. doi: 10.1109/TMTT.2009.2025429.

[10] M. Bozzi, A. Georgiadis, and K. Wu, "Review of substrate-integrated waveguide circuits and antennas," *IET Microw. Antennas Propag.*, vol. 5, no. 8, pp. 909-920, Jun. 2011. doi: 10.1049/iet-map.2010.0463.

[11] Y. L. Zhang, W. Hong, K. Wu, J. X. Chen, and H. J. Tang, "Novel substrate integrated waveguide cavity filter with defected ground structure," *IEEE Trans. Microw. Theory Techn.*, vol. 53, no. 4, pp. 1280-1287, Apr. 2005. doi: 10.1109/TMTT.2005.845750.

[12] W. Shen, W. Y. Yin, and X. W. Sun, "Compact substrate integrated waveguide (SIW) filter with defected ground structure," *IEEE Microw. Compon. Lett.*, vol. 21, no. 2, pp. 83-85, Feb. 2011. doi: 10.1109/LMWC.2010.2091402.

[13] Z-C. Hao, J-X. Chen, X-P. Chen, and K. Wu, "Compact super-wide bandpass substrate integrated waveguide (SIW) filters," *IEEE Trans. Microw. Theory Techn.*, vol. 53, no. 9, pp. 2968-2977, Sep. 2005. doi: 10.1109/TMTT.2005.854232.

[14] L-S. Wu *et al.*, "A new type of periodically loaded half-mode substrate integrated waveguide and its applications," *IEEE Trans. Microw. Theory Techn.*, vol. 58, no. 4, pp. 882-893, Apr. 2010. doi: 10.1109/TMTT.2010.2042832.

[15] J. D. Ruiz, F. L. Martínez-Viviente, A. Alvarez-Melcon, and J. Hinojosa, "Substrate integrated waveguide (SIW) with Koch fractal electromagnetic bandgap structures (KFEBG) for bandpass filter design," *IEEE Microw. Compon. Lett.*, vol. 25, no. 3, pp. 160-162, Mar. 2015. doi: 10.1109/LMWC.2015.2390537.

[16] Y. D. Dong, T. Yang, and T. Itoh, "Substrate Integrated waveguide loaded by complementary split-ring resonators and its applications to miniaturized waveguide filters," *IEEE Trans. Microw. Theory Techn.*, vol. 57, no. 9, pp. 2211-2222, Sep. 2009. doi: 10.1109/TMTT.2009.2027156.

[17] K. Deng, Z. Guo, C. Li, and W. Che, "A compact planar bandpass filter with wide out-of-band rejection implemented by substrate integrated waveguide and complementary split-ring resonator," *Microw. Opt. Technol. Lett.*, vol. 53, no. 7, pp. 1483-1487, Jul. 2011. doi: 10.1002/mop.

[18] M. Danaeian, K. Afrooz, A. Hakimi, and A. R. Moznebi, "Compact bandpass filter based on SIW loaded by open complementary split-ring resonators", *Int. J. RF Microw. Comput.-Aided Eng.*, vol. 26, no.8, pp. 674-682, Oct. 2016. doi: 10.1002/mmce.21017.

[19] W. Cao, Z. Zhang, S. Li, and P. Liu, "Ka band-stop filter based on complementary split ring resonator and SIW resonators," in *Proc. 11th Int. Symp. Antennas, Propagation and EM Theory*, 2016, pp. 832-833.

[20] F. Farzami, and M. Norooziarab, "Experimental realization of tunable transmission lines based on single-layer SIWs loaded by embedded SRRs," *IEEE Trans. Microw. Theory techn.*, vol. 61, no. 8, pp. 2848-2857, Aug. 2013. doi: 101109/TMTT.2013.2271759.

[21] J. B. Pendry, A. J. Holden, D. J. Robbins, and W. J. Stewart, "Magnetism from conductors and enhanced nonlinear phenomena," *IEEE Trans. Microw. Theory Techn.*, vol. 47, no. 11, pp. 2075-2084, Nov. 1999. doi: 10.1109/22.798002.

[22] J. D. Baena, *et al.*, "Equivalent-circuit models for split-ring resonators and complementary split-ring resonators coupled to planar transmission lines," *IEEE Trans. Microw. Theory Techn.*, vol. 53, no. 4, pp. 1451-1461, Apr. 2005. doi: 10.1109/TMTT.2005.845211.

[23] A. Velez, F. Aznar, J. Bonache, M. C. Velazquez-Ahumada, J. Martel, and F. Martin, "Open complementary split ring resonators (OCSRRs) and their application to wideband CPW band pass filters," *IEEE Microw. Compon. Lett.*, vol. 19, no. 4, pp. 197-199, Mar. 2009. doi: 10.1109/LMWC.2004.827836.

[24] A. Vélez, F. Aznar, M. Durán-Sindreu, A. J. Bonache, and F. Martín, "Stop-band and band-pass filters in coplanar waveguide technology implemented by means of electrically small metamaterial-inspired open resonators," *IET Microw. Antennas Propag.*, vol. 4, no. 6, pp. 712-716, Jun. 2010. doi: 10.1049/iet-map.2009.0291.

[25] J. Martel, R. Marqués, F. Falcone, J. D. Baena, F. Medina, F. Martín, and M. Sorolla, "A new LC series element for compact bandpass filter design," *IEEE Microw. Compon. Lett.*, vol. 14, no. 5, pp. 210-212, May 2004. doi: 10.1109/LMWC.2009.2015490.

[26] J. Hinojosa, M. Rossi, A. Alvarez-Melcon, and F. L. Martínez-Viviente, "Half mode substrate integrated waveguide (HMSIW) notch filters using open ring resonators," in *Proc. Metamaterials,* 2017, pp. 460-462.

[27] J. Hinojosa, A. Saura-Ródenas, A. Alvarez-Melcon, and F. L. Martínez-Viviente, "Reconfigurable coplanar waveguide (CPW) and half-mode substrate integrated waveguide (HMSIW) band-stop filters using a varactor-loaded metamaterial-inspired open resonator," *Materials*, vol. 11, no. 1, pp. 39-55, Jan. 2018. doi: 10.3390/ma11010039.

[28] J. D. Ruiz, J. Hinojosa, and A. Alvarez-Melcon, "Microstrip notch filters based on open interconnected split ring resonators (OISRRs)," *Appl. Phys. A*, vol. 112, pp. 263-267, Aug. 2013. doi: 10.1007/s00339-013-7744-x.

[29] J. D. Ruiz, and J. Hinojosa, "Shunt series LC circuit for compact coplanar waveguide notch filter design," *IET Microw. Antennas Propag.*, vol. 8, no. 2, pp. 125-129, Jan. 2014. doi: 10.1049/iet-map.2013.0401.

[30] J. Hinojosa, A. Saura-Ródenas, A. Alvarez-Melcon, and F. L. Martínez-Viviente, "Electronically tunable microstrip bandstop filters using a varactor-loaded open ring resonator (VLORR)," *Appl. Phys. A*, vol. 123, pp. 477-482, Jul. 2017. doi: 10.1007/s00339-017-1094-z.
[31] W. H. Tu, and K. Chang, "Compact microstrip bandstop filter using open stub and spurline," *IEEE Microw. Compon. Lett.*, vol. 15, no. 4, pp. 268-270, Apr. 2005. doi: 10.1109/LMWC.2005.845739.
[32] N. I. Dib, G. E. Ponchak, and L. P. B. Katehi, "A theoretical and experimental study of coplanar waveguide shunt stubs," *IEEE Trans. Microw. Theory techn.*, vol. 41, no. 1, pp. 38-44, Jan. 1993. doi: 101109/22.210227.
[33] G. Macchiarella, C. tomasoni, E. Massoni, M. Bozzi, and L. Perregrini, "A novel class of Half-mode SIW filters with extracted poles," in *Proc. 47th European Microwave Conference*, 2017, pp. 807-810. doi: 10.23919/EuMC.207.8230967.
[34] F. Falcone, T. Lopetegi, J.D. Baena, R. Marqués, F. Martín, and M. Sorolla, "Effective negative-ε stopband microstrip lines based on complementary split-ring resonators," *IEEE Microw. Compon. Lett.*, vol. 14, no. 6, pp. 280-282, Jun. 2004. doi: 10.1109/LMWC.2004.828029.
[35] A. Ebrahimi, W. Withayachumnankul, S. F. Al-Sarawi, and D. Abbott, "Compact second-order bandstop filter based on dual-mode complementary split-ring resonator," *IEEE Microw. Compon. Lett.*, vol. 26, no. 8, pp. 571-573, Aug. 2016. doi: 10.1109/LMWC.2016.2585544.
[36] J. García-García *et al.*, "Microwave filters with improved stopband based on sub-wavelength resonators," *IEEE Trans. Microw. Theory techn.*, vol. 53, no. 6, pp. 1997-2006, Jun. 2005. doi: 101109/TMTT.2005.848828.
[37] Kim, C. S. Cho, and J. W. Lee, "CPW bandstop filter using slot-type SRRs," *Electron. Lett.*, vol. 41, no. 24, pp. 1333-1334, Nov. 2005. doi: 10.1049/el.20053306.
[38] M. S. A. Rani, S. K. A. Rahim, M. R. Kamarudin, T. Peter, S. W. Cheung, and B. M. Saad, "Electromagnetic behaviors of thin film CPW-fed CSRR loaded on UWB transparent antenna," *IEEE Antennas Wireless Propag. Lett.*, vol. 13, pp. 1239-1242, 2014. doi: 10.1109/LAPWP.2014.2332514.
[39] V. Oznazi, and V. B. Erturk, "A comparative investigation of SRR- and CSRR-based band-reject filters: simulation, experiments, and discussions," *Microwave Opt. Technol. Lett.*, vol. 50, no. 2, pp. 519-523, Feb. 2008. doi: 10.1002/mop.23119.
[40] F. Falcone, F. Martín, J. Bonache, M. A. G. Laso, J. García-García, J. D. Baena, R. MArqués, and M. Sorolla, "Stop-band and band-pass characteristics in coplanar waveguides coupled to spiral resonators," *Microwave Opt. Technol. Lett.*, vol. 42, no. 5, pp. 386-388, Sep. 2005. doi: 10.1002/mop.20312.
[41] R. Torres-Torres, G. Romo, B. Horine, A. Sánchez, and H. Heck, "Full characterization of substrate integrated waveguides from S-parameter measurements," in *Proc. Electrical Performance of Electronic Packaging*, 2006, pp. 277-280. doi: 10.1109/EPEP.2006.321154.
[42] G. Doménech-Asensi, J. Hinojosa, J. Martínez-Alajarín, and J. Garrigós-Guerrero, "Empirical model generation techniques for planar microwave components using electromagnetic linear regression models," *IEEE Trans. Microw. Theory Techn.*, vol. 53, no. 11, pp. 3305-3311, Nov. 2005. doi: 101109/TMTT.2005.857331.
[43] D. Deslandes, "Design equations for tapered microstrip-to-substrate integrated waveguide transitions," in *Proc. IEEE MTT-S Int. Microw. Symp. Dig.,* 2010, pp. 704-707. doi: 10.1109/MWSYM.2010.5517884.
[44] E. Hammerstad and O. Jensen, "Accurate models for microstrip computer-aided design," in *Proc. IEEE MTT-S Int. Microw. Symp. Dig.,* 1980, pp. 407-409. doi: 10.1109/MWSYM.1980.1124303.

Juan Hinojosa was born in Dunkerque, France, in 1965. He received the Diplôme d'Etudes Approfondies (DEA) and the Ph.D. degree in electronics from Université des Sciences et Technologies de Lille (USTL), Lille, France, in 1990 and 1995, respectively.

In 1990, he joined the Hyper-frequency and Semiconductor Department of the Nanotechnologies and Microelectronics, Electronics Institute, as a Research Student, where he was involved in the development of electromagnetic characterization techniques of materials in microwave frequency range. Since 1999, he currently develops his teaching and research activities at the Universidad Politécnica de Cartagena, Cartagena, Spain. His research interests include characterization techniques of materials in microwave frequency range, development of novel microwave devices and modeling techniques for the design of microwave devices.

Marcello Rossi, photograph and biography not available at the time of publication.

Adrian Saura-Ródenas, photograph and biography not available at the time of publication.

Alejandro Álvarez Melcón (M'99–SM'07) was born in Madrid, Spain, in 1965. He received the Telecommunications Engineer degree from the Technical University of Madrid (UPM), Madrid, Spain, in 1991, and the Ph.D. degree in electrical engineering from the Swiss Federal Institute of Technology, Lausanne, Switzerland, in 1998.

In 1988, he joined the Signal, Systems and Radiocommunications Department, UPM, as a research student, where he was involved in the design, testing, and measurement of broad-band spiral antennas for electromagnetic measurements support (EMS) equipment. From 1991 to 1993, he was with the Radio Frequency Systems Division, European Space Agency (ESA/ESTEC), Noordwijk, The Netherlands, where he was involved in the development of analytical and numerical tools for the study of waveguide discontinuities, planar transmission lines, and microwave filters. From 1993 to 1995, he was with the Space Division, Industry Alcatel Espacio, Madrid, Spain, and was also with the ESA, where he collaborated in several ESA/European Space Research and Technology Centre (ESTEC) contracts. From 1995 to 1999, he was with the Swiss Federal Institute of Technology, École Polytechnique Fédérale de Lausanne, Lausanne, where he was involved with the field of microstrip antennas and printed circuits for space applications. In 2000, he joined the Technical University of Cartagena, Spain, where he is currently developing his teaching and research activities.

Dr. Álvarez Melcón was de recipient of the *Journée Internationales de Nice Sur les Antennes* (JINA) Best Paper Award for the best contribution to the JINA'98 International Symposium on Antennas, and the Colegio Oficial de Ingenieros de Telecomunicación (COIT/AEIT) Award to the best Ph.D. dissertation in basic information and communication technologies.

Félix Lorenzo Martínez Viviente was born in Cartagena (Spain) in 1972. He obtained his degree in Physics in 1995 and his Ph.D. in 2000 from Universidad Complutense de Madrid. During his thesis work he investigated the properties of hydrogenated silicon nitride thin films as a high-k dielectric for the gate of CMOS transistors. After completion of the PhD work he moved to the Universidad Politécnica de Cartagena, where he continued working on other high-k dielectrics (hafnium oxide) as well as other topics related to semiconductor physics and high frequency devices (gallium nitride HFETs, photonic and electromagnetic bandgap structures, and lead-free ferroelectric materials). He has extensive teaching experience in graduate and postgraduate courses on semiconductor physics, microelectronic devices, and photonics.